



Fatigue crack initiation and propagation in lotus-type porous material

S. Glodež, S. Dervarič, J. Kramberger

University of Maribor, Faculty of Mechanical Engineering, Smetanova 17, 2000 Maribor, Slovenia
srecko.glodez@um.si, saso.dervaric@student.um.si, janez.kramberger@um.si

M. Šraml

University of Maribor, Faculty of Civil Engineering, Smetanova 17, 2000 Maribor, Slovenia
matjaz.sraml@um.si

ABSTRACT. The investigation of fatigue strength of lotus-type structure with nodular cast iron as a base material using computational model is analysed in present study. The irregular pores distribution in transversal and longitudinal direction, regarding the external loading, is considered in the computational models. The complete fatigue process of analyzed porous structure is then divided into the crack initiation (N_i) and crack propagation (N_p) period where the total fatigue life (N) is defined as: $N = N_i + N_p$. The crack initiation period is determined using strain life approach where elastic-plastic numerical analysis is performed to obtain the total strain amplitude in the critical stress fields around the pores. The simplified universal slope method is then used to determine the number of stress cycles, N_i , required for formation of initial cracks. The number of stress cycles, N_p , required for crack propagation from initial to the critical crack length is also numerically determined using finite element (FE) models, in the frame of Abaqus computation FEM code. The maximum tensile stress (MTS) criterion is considered when analyzing the crack path inside the porous structure. The performed computational analyses show that stress concentrations around individual pores are higher when external loading is acting in transversal direction in respect to the pore distribution. Therefore, further computational analyses regarding crack initiation and crack propagation period have been done only for pores distribution in transversal direction.

KEYWORDS. Lotus-type porous structures; Fatigue crack initiation; Fatigue crack propagation; Numerical analysis.

INTRODUCTION

Generally, metal foams are relatively new class of materials with low densities and novel physical, mechanical, thermal, electrical and acoustic properties [1-5]. These materials offer potential for light-weight structures, energy absorption, sound absorption, etc. Therefore, metal foam materials present a unique opportunity for adoption in engineering applications. The base metals (aluminium, steel, etc.) are well understood and in many cases readily modelled with a high degree of accuracy. Foaming the metal, i.e. introducing voids in the microstructure, decreases the density and increases the apparent thickness. A number of distinct process-routes have been developed to make metal foams. Some of them produce open-cell foams and others produce foams in which majority of cells are closed.

Applications may at first be highly specialized, but as commercially material production volume increases, and costs decrease, widespread adoption of steel foams becomes possible [6]. Metal foams are frequently defined as either open or closed celled. Open-cell foam is comprised of only cell edges, so that open spaces exist between adjoining cells. Conversely, closed-cell foams are defined by solid faces so that each cell is closed off from those adjacent to it (Fig. 1).

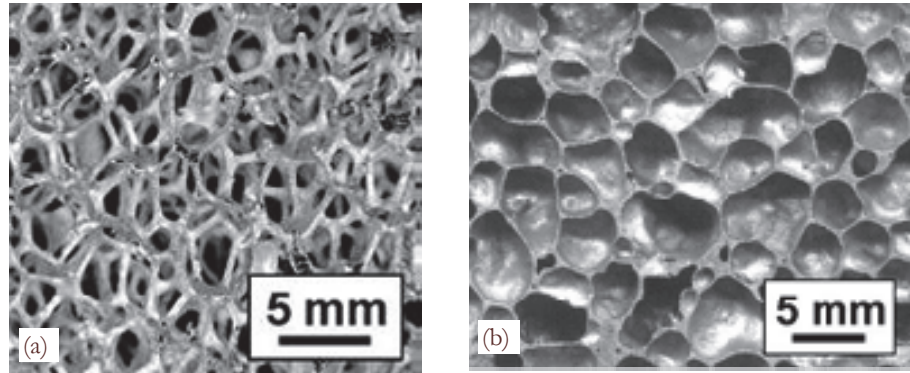


Figure 1: Open-cell (a) and closed-cell (b) of metal foam [6].

The characteristics of a foam are primarily determined by the material of which it is made, its relative density, ρ/ρ_s (the foam density, ρ , divided by that of the solid material of the cell wall, ρ_s), and by whether it has open or closed cells. Much of the research performed has presented the mechanical properties of foam as a function of the material's relative density. It is possible for foams with identical relative densities to have differing cellular structure or alternative ligament geometry which could significantly influence the behaviour and properties of the material [7, 8]. Metal foams can also be classified according to their porosity, or the number of cells (pores) that exist per unit length. Foams with the same relative density but a larger number of pores per unit length will contain ligaments with smaller cross sections as a greater number of pores and thus more ligaments will exist.

Lotus-type is a new type of porous material which comprises unidirectional pores. This makes the lotus-type materials very useful for application in lightweight structures, medicine, automotive engineering, sports equipment, etc. [9]. The porosity of lotus metals is usually lower than 70%, which is lower if compare to some conventional porous metals where porosity is often higher than 70% [10]. Moreover, pores of lotus-type metals are cylindrical, where the length of pores is usually large if compare to pore diameter (Fig. 2). Since the stress field around the pores depends on the loading direction, the relative high level of anisotropy is typical for lotus-type materials. While uniform stress distribution appears in the case when loading is acting along longitudinal direction of pores, the relative high stress concentration around the pores is characteristic for the perpendicular loading direction.

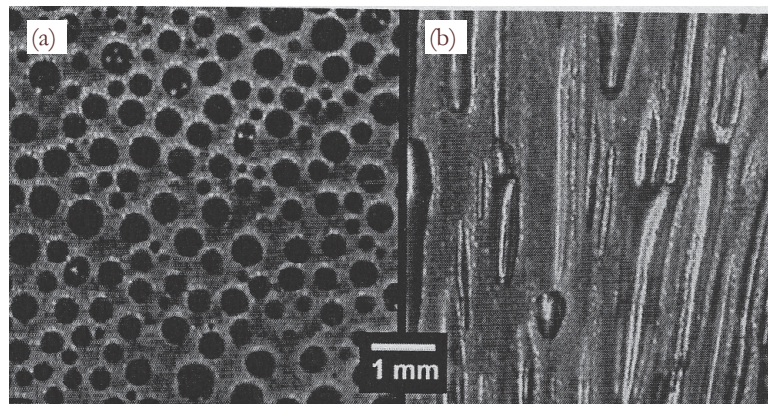


Figure 2: Cross section of lotus-type porous iron in transversal (a) and longitudinal (b) direction [9].

When porous material is used as a structural element, the fatigue behaviour of such porous structure should be known. Some investigations regarding fatigue behaviour of aluminium porous structures have been reported in [11-13]. However,



these results cannot be used for lotus-type porous materials due to different pore shapes and their orientations. Seki et al [10, 14, 15] have been studied the fatigue behaviour of cooper and magnesium lotus-type porous structures where the effect of porosity, anisotropic pore structure, and pore size distribution have been taken into account. Their experimental research has shown that for the fatigue loading parallel to the longitudinal axis of pores the stress field in the matrix is homogeneous and slip bands appear all over the specimen surface. This is not the case for transverse loading, where stress field is inhomogeneous and slip bands are formed only around pores because of high stress concentration in this region. Lately, some research works on metal foams have already been done at the University of Maribor [16-18]. However, these materials have not been fully characterized yet, particularly in the way of fatigue life behaviour.

In the presented paper, the fatigue process of lotus-type material is divided into the crack initiation and crack propagation period, where the total service life of treated structural element is defined as:

$$N = N_i + N_p \quad (1)$$

where N_i is the number of loading cycles required for the fatigue crack initiation and N_p is the number of loading cycles required for the crack propagation from initial to the critical crack length when final fracture can be expected to occur.

When determining the crack initiation period N_i , the strain life approach with consideration of simplified universal slope method [19] has been used

$$\varepsilon_a = 0.623 \cdot \left(\frac{R_m}{E} \right)^{0.832} \cdot (2N_i)^{-0.09} + 0.0196 \cdot (\varepsilon_f)^{0.155} \cdot \left(\frac{R_m}{E} \right)^{-0.53} \cdot (2N_i)^{-0.56} \quad (2)$$

where ε_a is the total strain amplitude, R_m is the ultimate tensile strength, E is the modulus of elasticity and ε_f is the true fracture strain. It is evident from Eq. (2) that the two exponents are fixed for all metals and that only monotonic material properties R_m , E and ε_f control the fatigue behavior.

The crack propagation period is in this paper described using simple Paris equation

$$\frac{da}{dN} = C \cdot \Delta K^m \quad (3)$$

where da/dN is the crack growth rate, ΔK is the stress intensity factor range ($\Delta K = K_{\max} - K_{\min}$), and C and m are the material parameters which are determined experimentally according to the load ration $R = K_{\min}/K_{\max}$ (the value $R=0.1$ has been considered in this study). The number of loading cycles N_p required for the crack propagation from initial crack length a_i to the critical crack length a_c can then be determined with integration of Eq. (3):

$$\int_0^{N_p} dN = \frac{1}{C} \int_{a_i}^{a_c} \frac{da}{\Delta K(a)} \quad (4)$$

COMPUTATIONAL MODEL

In some previous researches [9, 18], the regular models with aligned or for some angle aligned pores have been used when determining the strength behavior of lotus-type porous material. In these studies, the used computational models are built of multiple representative volume elements (RVEs) which are presented by a square block with central cylindrical hole of diameter d . The porosity of such structure is then regulated with change of pore diameters by keeping the size of the RVEs as a constant value [9]. In presented study, the irregular pores distribution of lotus-type material is considered. Pore distribution in transversal and longitudinal direction is assumed, respectively. A special image recognition code was developed, which was used to convert the chosen lotus-type material cross section image into the CAD-model which is then used to create the appropriate numerical model. The transverse computational model by square cross section of treated porous structure with length of 3.3 mm and randomly distributed pores with minimum and maximum diameters $d_{\min} = 0.084$ mm and $d_{\max} = 0.47$ mm, is introduced, respectively (Fig. 3 (a)). For such pores distribution, the porosity is equal to 36 %. The longitudinal computational model (Fig. 3(b)) is obtained as a cut section of

transverse model, where it was assumed that the average ratio $l/d \approx 15$ (l is the pore length and d is the pore diameter). Because the length of pores is larger as the pore diameter, the plain strain conditions was considered in the case for transversal loading regarding to pore distribution. On the other hand, the plain stress condition was assumed in the case, when loading appears in the longitudinal direction of pores. The boundary conditions are presented as displacement value of 0.01 mm at the top and fixed restraints in the bottom of used computational model (Fig. 3 (a) and (b)).

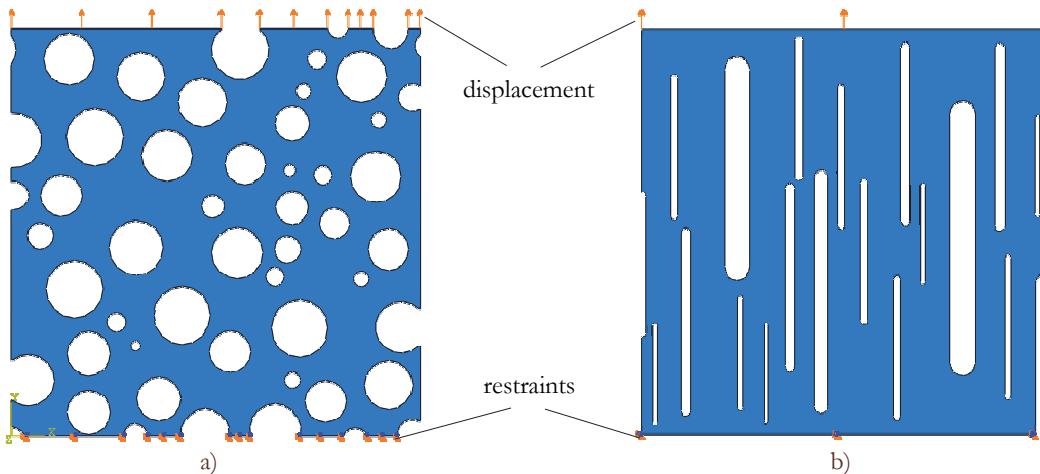


Figure 3: 2D computational model for pores distribution in transversal (a) and longitudinal (b) direction.

In performed computational analyses the lotus-type structure is made of nodular cast iron EN-GJS-400-18-LT as a base material, with monotonic material properties presented in Tab. 1. The true stress-strain behavior of material (Fig. 4), which is needed for determining the crack initiation period N_i , is assumed.

Yield stress R_e [MPa]	Ultimate tensile stress R_m [MPa]	True fracture strain ε_f [-]	Modulus of elasticity E [MPa]	Poisson's ratio ν [-]
256	417	0.235	$1.82 \cdot 10^5$	0.33

Table 1: Monotonic material properties of nodular cast iron EN-GJS-400-18-LT [20].

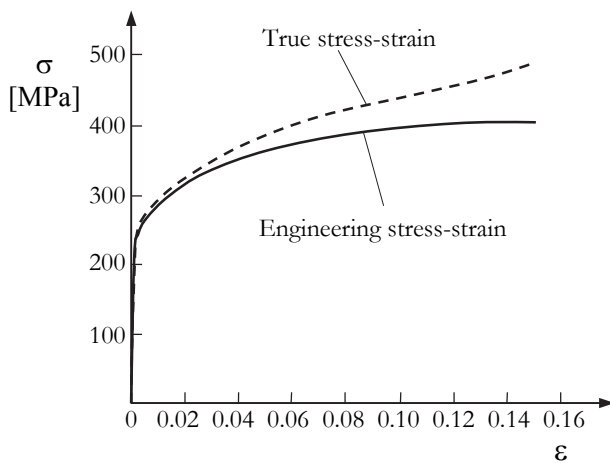


Figure 4: True stress-strain curve of base material [20]



NUMERICAL ANALYSIS

All computational models were discretized with quadratic finite elements with linear interpolation. Previous verification of required finite element size has also been done in respect to the results convergence with relative error 0.05. Fig. 5 shows the FE-mesh for both, transversal (Fig. 5 (a)) and longitudinal (Fig. 5 (b)) pores distribution.

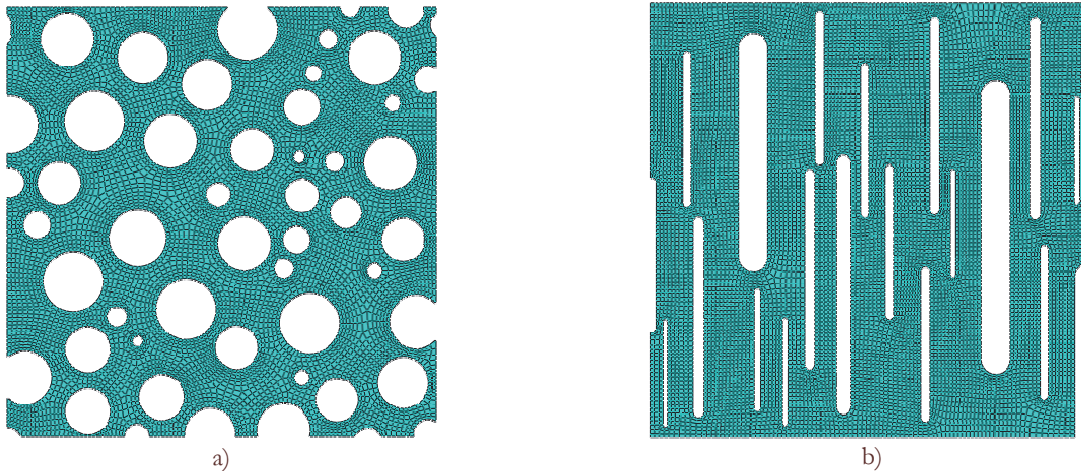


Figure 5: FE-mesh for pores distribution in transversal (a) and longitudinal (b) direction.

Crack initiation period for pores distribution in transversal direction

When studying the crack initiation period, the stress field around individual pores and location of the maximum stress concentration should be determined first. The maximum von Mises equivalent stress $\sigma_M = 350$ MPa with the appropriate total strain $\varepsilon = 0.022$ are recognized in a cross section No. 1 (Fig. 6 (a)). Considering the pulsating loading ($\varepsilon_a = \varepsilon/2 = 0.011$) and material properties as presented in Tab. 1, the number of loading cycles N_i required for the fatigue crack initiation is then calculated according to Eq. (2). In the next step, the initial crack $a_i = 0.05$ mm is added into the critical cross section No. 1 (Fig. 6 (b)) and the numerical procedure is continued with the crack propagation period. When the fatigue crack reaches the critical length, the complete fracture of cross section No. 1 occurs which mean that two neighboring pores are connected with a seam and the complete procedure is repeated regarding to the other critical cross section.

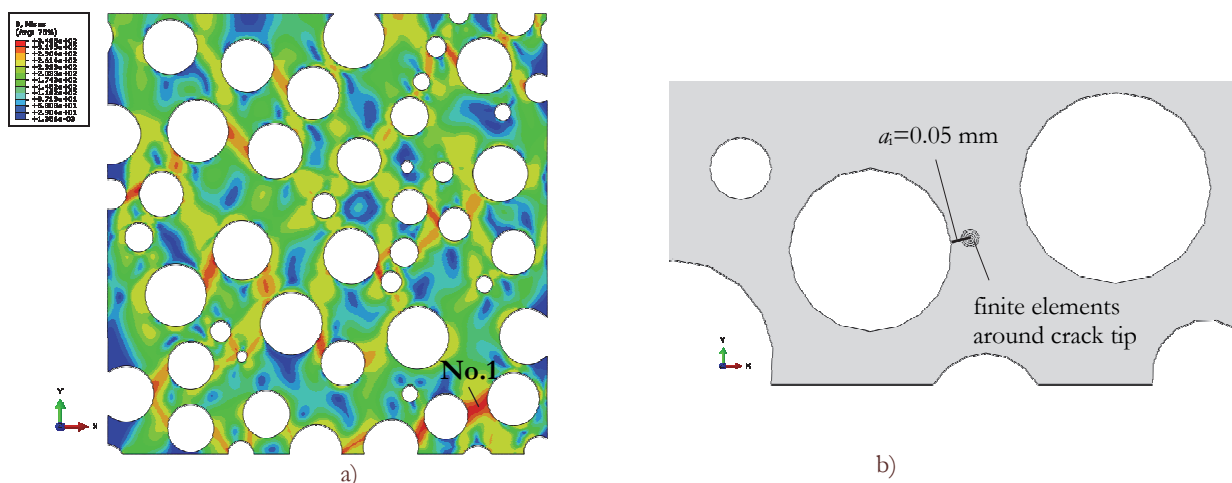


Figure 6: Schematic procedure of crack initiation period. (a) maximum stress concentration in a cross section No. 1 (b) initial crack in a cross section No. 1.

Crack propagation period for pores distribution in transversal direction

The crack initiation period of each critical cross section is finished with the formation of initial crack of length a_i after the appropriate number of stress cycles N_i . The crack propagation period is then analyzed using Paris Eq. (3), where the following material parameters have been considered [20]:

$$C = 4.608 \cdot 10^{-12} \frac{\text{m/cycle}}{(\text{MPa}\sqrt{\text{m}})^{3.86}}; \quad m = 3.86; \quad \Delta K_{\text{th}} = 20.8 \text{ MPa}\sqrt{\text{m}}; \quad \Delta K_{\text{lc}} = 30.4 \text{ MPa}\sqrt{\text{m}}$$

Than, the stress intensity factor is determined numerically using Abaqus FEM software, where the equivalent stress intensity range ΔK_{eq} as a combined value of mixed mode conditions ΔK_I and ΔK_{II} has been considered. To analyse the fatigue crack growth under mixed mode conditions the value ΔK in Eq. (3) has to be replaced with the value ΔK_{eq} . The crack propagation angle is in each calculating step determined using maximum tensile stress (MTS) criterion. The analysis of crack propagation has been stopped when the equivalent stress intensity factor range ΔK_{eq} exceeded the critical value ΔK_{lc} or when the crack reached the vicinity of neighboring pore. At that moment it was assumed that two neighboring pores are connected with a seam and the computational procedure was continued with the crack initiation period in other critical cross section. Fig. 7 shows the numerical procedure of crack propagation in a cross section No. 1.

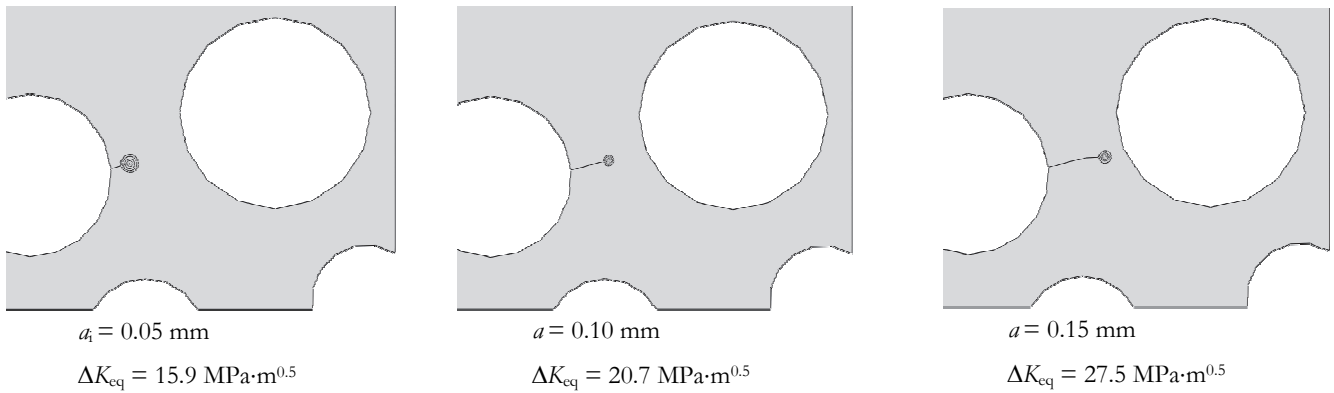


Figure 7: Schematic procedure of crack propagation period in a cross section No. 1.

Crack initiation and propagation period for pores distribution in longitudinal direction

When studying the case of pores distribution in longitudinal direction, more homogenous stress and deformation field has been found around the longitudinal pores. This finding is also in agreement with the experimental work published in [10] where authors have pointed out that the stress concentration around the pores is in the case of longitudinal pores lower if compare to the transversal pore distribution. Therefore, the crack initiation and crack propagation period for longitudinal pore distribution has not been studying in the framework of this paper. It was assumed that the fatigue life for crack initiation and further for crack propagation until critical crack length would be much longer if compared to the treated calculation for transversal pores distribution.

COMPUTATIONAL RESULTS AND DISCUSSION

Fig. 8 shows the numbering of critical cross sections where both, crack initiation and crack propagation period have been studied. The maximum stress concentration appeared first in cross section No. 1 where initial failure occurred after certain number of stress cycles ($N_i = 472$ cycles for formation of initial crack of length $a_i = 0.05$ mm and $N_p = 212$ cycles for this initial crack to propagate until critical length $a_c = 0.15$ mm). Thereafter, the complete computational procedure is repeated in a cross section No. 2, where the maximum stress concentration occurred in the next calculating step. Here, the seam between neighboring pores in a cross section No. 1 is considered during the numerical analyses. As shown in Fig. 8, seven subsequent cross sections have been analyzed in respect to the crack initiation and crack propagation period in treated lotus-type porous structure with pore distribution in transversal loading



direction. The final computational results are presented in Tabs. 2 and 3, while the crack path is shown in Fig. 9, where scale factor 10 is used. It is evident from Fig. 9, that complete fracture of upper left half structure is expected after cross section No. 7 will be broken. The appropriate total number of stress cycles N according to Eq. (1) can then be assumed as a total fatigue life of treated structure.

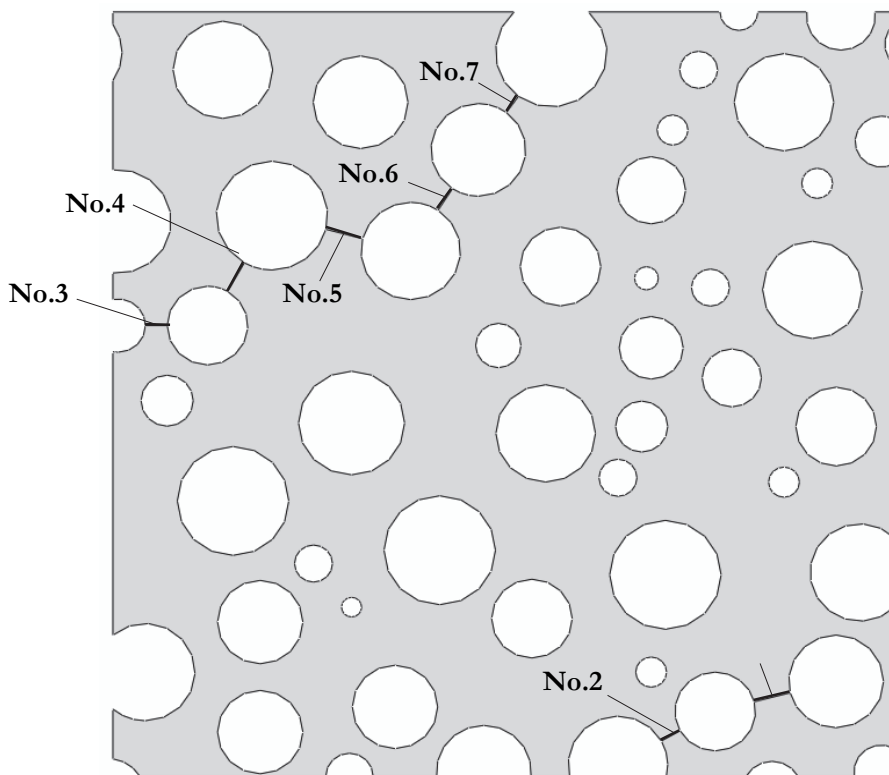


Figure 8: Numbering of critical cross sections

Cross section No.	Von Mises equivalent stress σ_M [MPa]	Total strain amplitude ϵ_a [MPa]	Crack initiation period N_i [cycles]	Initial crack length a_i [mm]
1	350	0.0110	472	0.05
2	378	0.0229	110	0.03
3	344	0.0136	307	0.03
4	336	0.0121	387	0.03
5	327	0.0108	489	0.03
6	326	0.0200	495	0.03
7	304	0.0090	731	0.03

Table 2: Computational results for the crack initiation period.

CONCLUSIONS

The computational fatigue strength investigation in respect to the crack initiation and crack propagation in dynamic loaded lotus-type porous structure made of nodular cast iron is presented in this paper. The crack initiation period, N_i , has been determined using strain life approach with consideration of simplified universal slope method

to determine the number of stress cycles N_i required for formation of initial cracks. The crack propagation period, N_p , has been determined using Paris equation, where the relationship between the stress intensity factor and crack length has been determined numerically using Abaqus-software. Here, the MTS-criterion has been considered when analyzing the crack path inside the lotus-type porous structure. The crack initiation and crack propagation period have been studied in seven subsequent critical cross sections between different pores as shown in Fig. 8. The total fatigue life, N , of the lotus-type porous structure under given boundary conditions has then been determined as a sum of N_i and N_p for all considered cross sections.

Cross section No.	Initial crack length a_i [mm]	Critical crack length a_c [mm]	Function $\Delta K_{eq} = f(a)$	Crack propagation period N_p [cycles]
1	0.05	0.15	$4E+08a^2+35734a+13.171$	212
2	0.03	0.09	$1E+09a^2+40056a+14.989$	113
3	0.03	0.09	$1E+09a^2+115195a+6.629$	350
4	0.03	0.19	$-4E+08a^2+139479a+6.189$	1109
5	0.03	0.13	$3E+08a^2+113530a+12.203$	162
6	0.03	0.13	$-5E+08a^2+119507a+10.049$	519
7	0.03	0.11	$-5E+07a^2+17932a+11.267$	1099

Table 3: Computational results for the crack propagation period.

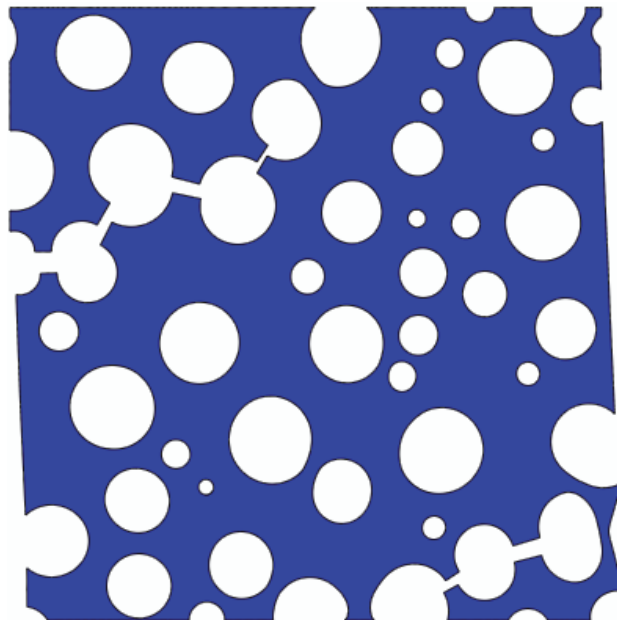


Figure 9: Crack path in the lotus-type porous structure

Computational results for the pores distribution in the transversal direction have shown that the number of stress cycles for the crack initiation in the individual cross sections varied between 307 and 731, while the number of stress cycles for the crack propagation until final breakage of individual cross section varied between 113 and 1109, which correspond to the regime of low cycle fatigue. Computational results have also shown that quite uniform stress distribution appears in the case when loading is acting along longitudinal direction of pores. Therefore, the appropriate longer fatigue life could be expected in that case.



In the framework of further research work, the eXtended Finite Element Method (XFEM) numerical procedure implemented in Abaqus code could be used to study the fatigue behavior of treated porous structure. The main advantage of such procedure would be simultaneous fatigue analyses of different cross sections which was not the case in present study. Furthermore, the real experimental procedure on real lotus-type porous structures will be needed to confirm the computational results.

REFERENCES

- [1] Ashby, M.F., Evans, A., Fleck, N.A., Gibson, L. J., Hutchinson, J. W., Wadley, H. N. G., Metal Foams: A Design Guide. Butterworth-Heinemann, Woburn, (2000).
- [2] Harte, A.M., Fleck, N.A., Ashby, M.F., Fatigue failure of an open cell and a closed cell aluminium alloy foam, *Acta Materialia*, 47(8) (1999) 2511-2524.
- [3] Ingraham, M.D., De Maria, C.J., Issen, K.A., Morisson, D.J., Low cycle fatigue of aluminium foam, *Materials Science and Engineering A*, 504 (2009) 150-156.
- [4] Patrick, J. V., Investigation of the behaviour of open cell aluminium foam, MSc. thesis, University of Massachusetts - Amherst, (2010).
- [5] Pinto, H., Arwade, S. R., Veale, P., Response of open cell aluminium foams to fully reversed cyclic loading, *Journal of Engineering Mechanics*, 137(12) (2011) 911-918.
- [6] Smith, B.H., Szyniszewski, S., Hajjar, J.F., Schafer, B.W., Arwade, S.R., Steel foam for structures: A review of applications, manufacturing and material properties, *Journal of Constructional Steel Research*, 71 (2012) 1-10.
- [7] Redenbach, C., Microstructure models for cellular materials, *Computational Materials Science*, 44 (2009) 1397-1407.
- [8] Altenbach, H., Öchsner, A., Cellular and porous materials in structures and processes, CISM courses and lectures, Springer Verlag, Wien-NewYork, 521 (2010).
- [9] Vesenjak, M., Kovačić, A., Masakazu, T., Borovinšek, M., Nakajima, H., Ren, Z., Compressive properties of lotus-type porous iron, *Computational material science*, 65 (2012) 37-43.
- [10] Seki, H., Tane, M., Nakajima, H. Fatigue crack initiation and propagation in lotus-type porous copper, *Materials transactions*, 49 (2008) 144-150.
- [11] Amsterdam, E., De Hosson, J.M., Onck, P.R., Failure mechanisms of closed-cell aluminium foam under monotonic and cyclic loading, *Acta Mater.*, 54 (2006) 4465-4472.
- [12] Olurin, O.B., McCullough, K.Y.G., Fleck, N.A., Ashby, M.F., Fatigue crack propagation in aluminium's alloy foams, *Int. J. Fatigue*, 23 (2001) 375-4472.
- [13] Zhou, J., Soboyejo, W. O., An investigation of deformation mechanisms in open cell aluminum foams, *Materials Science and Engineering*, A386 (2004) 118-128.
- [14] Seki, H., Tane, M., Nakajima, H., Effects of Anisotropic Pore Structure and Fiber Texture on Fatigue Properties of Lotus-type Porous Magnesium, *J. Mater. Res.*, 22(11) (2007) 3120-3129.
- [15] Seki, H., Tane, M., Otsuka, M., Nakajima, H., Effects of Pore Morphology on Fatigue Strength and Fracture Surface of Lotus-type Porous Copper, *J. Mater. Res.*, 22(7) (2007) 1331-1338.
- [16] Vesenjak, M., Borovinšek, M., Fiedler, T., Higa, Y., Ren, Z., Structural characterization of advanced pore morphology (APM) foam elements. *Materials letters*, 110 (2013) 201-203.
- [17] Vesenjak, M., Krstulović-Opara, L., Ren, Z., Characterization of irregular open-cell cellular structure with silicone pore filler, *Polymer testing*, 32 (2013) 1538-1544.
- [18] Vesenjak, M., Ren, Z., Öchsner, A., Dynamic behavior of regular closed-cell porous metals - computational study, *International journal of materials engineering innovation*, 1 (2009) 175-196.
- [19] Muralidharan, U., Manson, S.S., Modified universal slope equation for estimation of fatigue characteristics, *Trans. ASME, J. Eng. Mater. Tech.*, 110 (1988) 55-88.
- [20] Čanžar, P., Tonković, Z., Drvar, N., Bakić, A., Kodvanj, J., Sorić, J., Experimental investigation and modelling of fatigue behavior of nodular cast iron for wind turbine applications, *Proceedings of EURODYN 2011*, Leuven, Belgium, (2011) 3252-3257.